# Electrochemical Atomic Force Microscopy Using a Tip-Attached Redox Mediator for Topographic and Functional Imaging of Nanosystems

**Agnès Anne,[†] Edmond Cambril,[‡] Arnaud Chovin,[†] Christophe Demaille,[†,*] and Cédric Goyer[†]**

[†]Laboratoire d'Electrochimie Moléculaire, Unité Mixte de Recherche Université, CNRS No. 7591, Université Paris Diderot, Paris 7, 15 rue Jean-Antoine de Baïf, 75205 Paris Cedex 13, France, and [‡]Laboratoire de Photonique et de Nanostructures (LPN/CNRS), Route de Nozay, 91460 Marcoussis, France

**ABSTRACT** We describe the development of a new type of high-resolution atomic force electrochemical microscopy (AFM-SECM), labeled Tarm (for tip-attached redox mediator)/AFM-SECM, where the redox mediator, a ferrocene (Fc), is tethered to the AFM-SECM probe *via* nanometer long, flexible polyethylene glycol (PEG) chains. It is demonstrated that the tip-attached ferrocene-labeled PEG chains effectively shuttle electrons between the tip and substrate, thus acting as molecular sensors probing the local electrochemical reactivity of a planar substrate. Moreover the Fc-PEGylated AFM-SECM probes can be used for tapping mode imaging, allowing simultaneous recording of electrochemical feedback current and of topography, with a vertical and a lateral resolution in the nanometer range. By imaging the naturally nanostructured surface of HOPG, we demonstrate that Tarm/AFM-SECM microscopy can be used to probe the reactivity of nanometer-sized active sites on surfaces. This new type of SECM microscopy, being, by design, free of the diffusional constraints of classical SECM, is expected to, in principle, enable functional imaging of redox nanosystems such as individual redox enzyme molecules.

**KEYWORDS:** electrochemical microscopy · SECM · electrochemical atomic force microscopy · AFM/SECM · tapping mode AFM/SECM · tip-attached redox mediator/electrochemical atomic force microscopy · Tarm/AFM-SECM · redox-functionalized AFM tips · HOPG electrochemistry

Scanning electrochemical microscopy (SECM) is a "near-field" electrochemical technique which is designed to probe the local reactivity of surfaces.[1−3] In a classical SECM configuration, a microelectrode, a few micrometers or even a few nanometers in size, is approached toward a substrate immersed in an electrolyte solution containing a soluble redox mediator. The microelectrode (tip or probe) is biased so as to oxidize or reduce the redox mediator. Providing the tip−substrate separation is made smaller than the microelectrode size, the tip-generated form of the mediator reaches the substrate surface by diffusion. There, the mediator is converted back to its initial redox form and fed back to the tip, thus increasing the tip−current in a so-called SECM positive feedback process. The dependence of the tip−current on the tip−substrate separation can then be used to characterize the kinetics of the electrochemical reaction taking place at the substrate surface.[1−3] By scanning the tip over the substrate at a fixed distance, while recording the electrochemical current, SECM can also be used to construct tip−current images, allowing the distribution of electroactive sites present over the surface of a composite substrate to be spatially resolved and their individual reactivity probed.[4−7] The lateral resolution of this functional imaging mode of SECM, defined as the size of the smallest surface sites which can be electrochemically resolved, is governed by the radius of the microelectrode: the respective sizes of the tip and of the redox-active sites have to approximately match for optimal feedback to be detected.[8] Consequently, with few exceptions,[9] most of the efforts aiming at increasing the resolution of SECM imaging have focused on decreasing the electrode size, and fabrication techniques allowing the production of SECM tips as small as a few tens of nanometers are now available.[10−14] In that size range, coupling of SECM with another near-field technique is often necessary to control the approach of the tip from the substrate. Atomic force microscopy (AFM) is often used to this aim.[15−27]

However, beyond technical constraints related to the fabrication of nanosized tips, probing the reactivity of a surface at the nanoscale by SECM is hampered by a fundamental limitation, identified at the early stage of the development of electrochemical microscopy[28,29] and recalled recently:[3] feedback SECM can only probe surface reactivity if the turnover of the surface reaction is fast enough with respect to the diffusion

*Address correspondence to demaille@univ-paris-diderot.fr.

Received for review March 9, 2009 and accepted September 12, 2009.

**Published online September 21, 2009.**
10.1021/nn9009054 CCC: $40.75

rate of the soluble redox mediator.[4,8,30] This diffusion rate is given by the time it takes for the mediator to diffuse from the tip to the surface, that is, to diffuse over a distance corresponding to a fraction of the tip radius. If the above limiting condition is not met, the mediator is carried away by spherical diffusion, no feedback process occurs, and the site is seen as unreactive. Therefore, increasing the lateral resolution of SECM by simply decreasing the microelectrode size leads to the following paradox: resolving small reactive sites on a surface requests small probes, but decreasing the probe size increases the rate of diffusion up to the point where "slowly" reacting sites become undetectable by SECM. This problem is particularly acute for functional probing of nanometer-sized surface sites; for example, on a ~10 nm length scale, a typical SECM soluble mediator, characterized by a diffusion coefficient of $\sim 10^{-5}$ $cm^2/s$, diffuses across the tip−substrate gap in ~0.1 μs, so that only reactive sites having a turnover higher than 10 $\mu s^{-1}$ can be probed at that scale. This limitation notably precludes the use of feedback SECM to access the reactivity of individual redox enzyme molecules, a very actively sought goal[31,32] since redox enzymes are typically ~10 nm in size and display a turnover in the ~microsecond time scale.[33]

In that context, we are presenting here an innovative electrochemical atomic force microscopy, free of the above-discussed diffusional constraints of classical SECM, and which is specifically designed to enable functional probing of nanosystems on surfaces. This new type of SECM microscopy, we label Tarm (for tip-attached redox mediator)/AFM-SECM, uses as SECM mediator a ferrocene moiety (Fc) tethered to an AFM-SECM probe *via* nanometer-sized, flexible polyethylene glycol (PEG) chains. The AFM-SECM configuration is meant to allow the tip-borne Fc-PEG chains to be brought in the vicinity of the reactive nanosites to be probed, where the Fc heads will react, and will be exhaustively collected back by the tip, instead of being dispersed by diffusion. Another benefit of attaching the mediator to the probe is that the lateral resolution of Tarm/AFM-SECM is expected to be governed by the size of the Fc-PEG chains, and not by the tip size like in classical SECM, and therefore to be in the nanometer range.

In a previous paper,[34] we described the fabrication of AFM-SECM tips bearing redox Fc-(PEG) chains and validated their use as Tarm/AFM-SECM probes on the basis of contact mode approach curves. The working principle of this innovative SECM microscopy was also established: it was shown that the tip-borne PEG chains are flexible enough to allow their Fc heads to efficiently "sense" locally the electrochemical reactivity of an homogeneous substrate. In the present paper, we demonstrate the capabilities of Tarm/AFM-SECM microscopy for high-resolution functional imaging of heterogeneous substrates presenting localized nanosites of differing electrochemical reactivities. In particular, we show that using Tarm/AFM-SECM in tapping mode allows one to simultaneous record topographical and electrochemical images of a model nanostructured substrate, HOPG, with a lateral resolution in the nanometer range.

## RESULTS AND DISCUSSION

**Fabrication and Characterization of AFM-SECM Probes Bearing Fc-PEG Chains.** Home-made AFM-SECM probes (tips) consisting in a bent gold microwire, flattened to act as a flexible cantilever, and bearing a very smooth spherical tip of submicrometer dimension were fabricated as described previously.[20] The probe is entirely insulated by deposition of electrophoretic paint, glued onto a standard AFM silicon chip, and its spherical tip end is selectively exposed in order to act as a current-sensing microelectrode. Functionalization of the gold spherical microelectrode was carried out by immersing the extremity of a combined probe into a drop of an aqueous solution containing ~0.5 mM of a custom-synthesized linear Fc-$PEG_{3400}$−disulfide molecules, made of poly(ethylene glycol) chains of 3400 molecular weight and bearing a redox ferrocene moiety head at each extremity, for ~2 h. This resulted in the covalent end-grafting of the Fc-PEG chains to the surface of the spherical tip end *via* a stable gold−sulfur bond, as represented in Scheme 1.

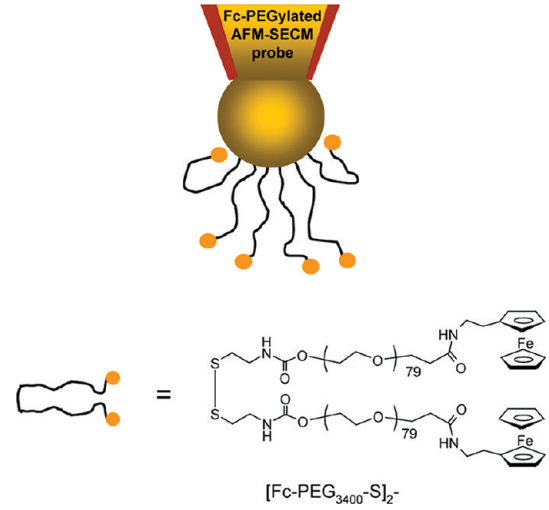


**Scheme 1. Depiction of the extremity of an AFM-SECM combined probed functionalized by the home-prepared Fc-$PEG_{3400}$−disulfide molecule,[34] yielding a Fc-PEGylated AFM-SECM probe (the scheme is not on scale).**

Fc-$PEG_{3400}$ chains were specifically chosen in the prospect of using Tarm/AFM-SECM to probe the kinetics of single redox enzyme molecules. Indeed, we previously demonstrated that Fc-$PEG_{3400}$ chains exhibited the necessary biocompatibility to convey electrons within integrated systems consisting of organized multilayers of a "model" redox enzyme, glucose oxidase, assembled onto an electrode.[35,36] In these systems, the PEG-borne Fc heads were able to reach the

prosthetic group of the enzyme, albeit deeply buried within the enzyme's catalytic pocket,[37] where they served as efficient cofactors. We also demonstrated that, when grafted onto a gold planar surface *via* a gold−sulfur linkage, Fc-$PEG_{3400}$ chains form robust layers.[38,39] In addition, we verified that, when these layers are probed by an incoming bare AFM-SECM tip, the chains display the required hydrophilicity and flexibility for their Fc heads to efficiently shuttle electrons from the substrate to the tip across nanometer-sized tip−substrate gap.[21,22]

The thus fabricated Fc-PEGylated probes were characterized as described previously,[34] using contact mode AFM-SECM, by approaching the probes toward a bare substrate in a 1 M $NaClO_4$ containing aqueous electrolyte solution. Analysis of the force approach curves allowed the chain coverage and conformation of the tip-grafted chains to be derived,[34] by making use of the theoretical force laws describing the compression of a layer of end-grafted linear polymers.[40−43] We found that the apex of the Fc-PEGylated probes is covered with a layer of Fc-PEG chains forming noninterpenetrating hemispherical blobs (or "mushrooms") of a size close to the Flory radius of the coiled chain in solution: $R_F \sim 5$ nm.

Using Tarm/AFM-SECM microscopy for functional imaging of a substrate implies being able to scan the substrate surface with the Fc-PEGylated probe, while maintaining a constant tip−substrate separation. In the present case, the tip−substrate separation should be such that the chains can efficiently shuttle electrons to/from the tip and from/to the substrate, that is, be such that a faradaic current is measured. Understandably, this distance should be in the order of the chain size (*i.e.*, of ∼5 nm).

In our preliminary work,[34] we showed that the forces between the Fc-PEGylated probe and the substrate are too weak to be used to maintain such a narrow tip−substrate separation for imaging purposes, as is classically done in contact mode force feedback AFM. Therefore, we decided to turn to tapping mode AFM. However, using tapping mode operation for Tarm/AFM-SECM microscopy raises a fascinating question, which is experimentally addressed below: can Fc-PEG chains grafted to an oscillating AFM-SECM tip efficiently probe the local electrochemical reactivity of a substrate?

**Tapping Mode AFM-SECM Using a Fc-PEGylated Probe: Amplitude and Current Approach Curves.** In tapping mode AFM, the tip is oscillated by mechanical excitation and the tip oscillation amplitude is used as the AFM feedback signal.[44] The dependence of the oscillation amplitude on the tip−substrate separation is therefore used to maintain the tip at a constant average altitude over the substrate. Moreover, since the tip solely comes in intermittent contact with the substrate, lateral frictional forces are minimized, which makes this technique ideally suited for imaging fragile biological species and very attractive as a basis for the microscopy we propose to develop. It is also worth noting that *in situ* tapping mode AFM has proved to be highly suitable for the structural characterization of molecular layers self-assembled onto surfaces[45,46] and was also used in a recent report for studying the compression of surface-immobilized PEG chains.[47]

Upon mechanical excitation by a dithering piezo, the home-fabricated AFM-SECM probes gave rise to multiple resonance peaks at frequencies ranging from 1 to 10 kHz. The drive frequency was chosen close to the resonance peak corresponding to the most stable imaging conditions, usually found in the ∼7−8 kHz region (see Supporting Information). The resulting typical free oscillation amplitude of the tip, $A_0$, recorded far away from the substrate, was in the 5−10 nm range.

In a typical experiment, a vibrating Fc-PEGylated AFM-SECM probe was approached toward a bare flat HOPG substrate in a 1 M $NaClO_4$ containing aqueous electrolyte solution. The Fc-PEGylated tip and substrate were, respectively, biased at potentials largely positive ($E_{tip} = +0.30$ V/SCE) and largely negative ($E_{sub} = -0.01$ V/SCE) with respect to the standard potential of the ferrocene head ($E° = +0.15$ V/SCE).[21] The amplitude of the tip vibration ($A$) and the tip−current ($i$) were recorded simultaneously and plotted as a function of the time-averaged tip−substrate separation $d$ (Figure 1, drive frequency = 8.66 kHz). In tapping mode operation, the tip oscillates symmetrically around its resting position so that $d$ is simply related to the imposed piezo elongation, $Z_{piezo}$ by $d = Z_{piezo} + Z_0$, where $Z_0$ is the piezo elongation corresponding to the hard contact between the probe and the HOPG substrate, derived from the approach curves as described in the Methods section. The instantaneous tip−substrate distance varies periodically from a maximum of $d_{max} = d + A$ down to a minimum distance of $d_{min} = d - A$, as sketched in the inset of Figure 1b.

The recorded combined amplitude−current approach curves presented in Figure 1 can be delineated into three zones (I, II, III):

***Zone I:*** ($d \gg 20$ nm) the tip−substrate separation is large enough for the Fc-PEGylated not to interact with the substrate. As a result, the amplitude is independent from the tip−substrate separation and corresponds to the free amplitude $A_0 \sim 7$ nm, and no current is recorded.

***Zone II:*** ($d \sim 3-20$ nm) upon further approach of the Fc-PEGylated probe toward the surface, the probe oscillation starts to be damped for $d \sim 22$ nm. Throughout zone II, the amplitude is such that $A < d$ so that there is no contact between the gold tip itself and the substrate. Damping is actually caused by intermittent contact between the tip-borne Fc-PEG chains and the substrate surface. The onset of damping corresponds to a closest tip−substrate separation during each oscillation cycle of $d_{min} = 22 - A_0 = 15$ nm. As sketched in the in-

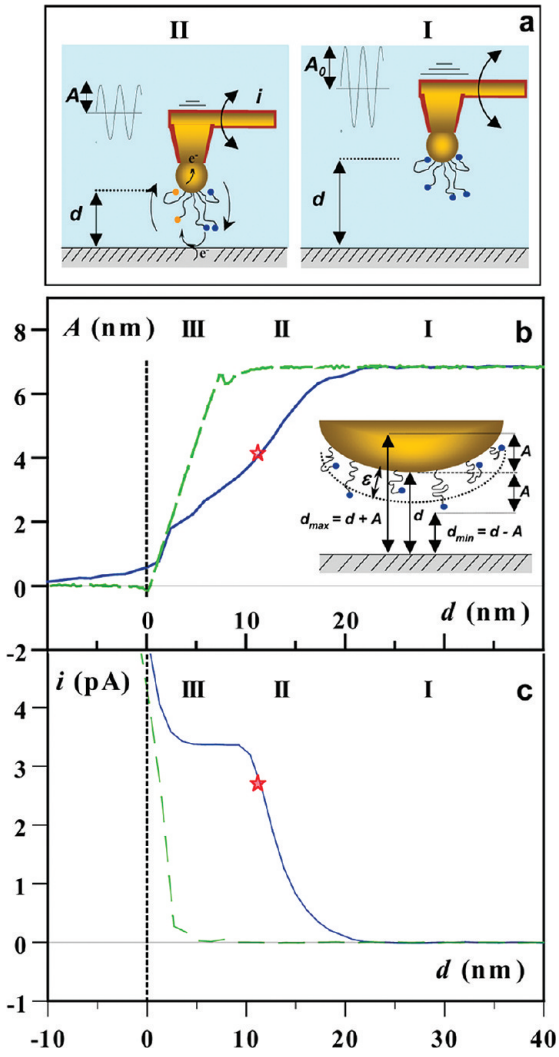


**Figure 1. Tapping mode AFM-SECM approach curves using a Fc-PEGylated probe. (a) Depiction of the behavior of the Fc-PEGylated AFM-SECM probe approaching a planar substrate: (I) Fc-PEGylated probe is oscillated by mechanical excitation; the probe is in solution, far away from the substrate, and its free oscillation amplitude is $A_0 \sim 7$ nm. (II) When the Fc-PEGylated probe is brought sufficiently close to the substrate, intermittent contact between the Fc-PEG layer and the substrate results in decreasing the tip oscillation amplitude to $A < A_0$. Concomitantly, the PEG-borne Fc heads contact the substrate surface, where they are oxidized, and are subsequently reduced at the tip, thus generating the SECM elastic bounded diffusion feedback current, *i*. (b) Amplitude and (c) tip−current approach curves simultaneously acquired upon approaching a Fc-PEGylated probe from a bare HOPG substrate (continuous lines). Also shown in (b) and (c), as green dashed lines, are the equivalent approach curves recorded using a bare AFM-SECM probe. The inset in (b) depicts the tip-borne Fc-PEG layer, characterized by a thickness ε, and also the average tip−substrate separation, *d*. During one oscillation cycle of the probe, the instantaneous tip−substrate distance varies periodically from a maximum of $d_{max}$ down to a minimum distance of $d_{min}$, as shown. The star symbol in (b) and (c) indicates the distance below which the Fc-PEG layer is permanently in contact with the substrate. Tip drive frequency: 8.66 kHz. The substrate potential $E_{sub}$ was held at −0.01 V/SCE, and the tip potential was $E_{tip}$ = +0.30 V/SCE; 1 M $NaClO_4$ supporting aqueous electrolyte. Approach rate: 5 nm/s.**

set of Figure 1, this value can be taken as being the effective thickness of the Fc-PEG layer, ε. We note that this ε value is comparable to, albeit larger than, $R_F$, the Flory radius of the chains. This is not unexpected because, for long end-grafted linear chains, the chain monomers are actually randomly distributed away from the anchoring surface (*i.e.*, here the tip), following a distribution profile which extends into solution over distances of a few times $R_F$.[22,48] In other words, $R_F$ is only the statistical dimension of the "blob" size formed by the anchored chain: monomers can be found away from the tip surface and obviously do contact the substrate, for $d_{min} > R_F$. As seen in Figure 1c, the same applies for chain heads since a current is also detected at the onset of damping, indicating that the tip-borne Fc heads start to electrochemically contact the substrate for $d_{min} = \varepsilon = 15$ nm. Considering that both *d* and *A* are determined here within an accuracy of ±1 nm, this value is in good agreement with the current onset value of ~12 nm, observed in contact mode current approach curves.[34] When *d* is further decreased, the amplitude decreases progressively, roughly following a S-shaped variation, which is reminiscent of amplitude approach curves recorded on elastomer surfaces.[49] Meanwhile, the recorded current increases smoothly, leveling off to an intensity of $i_{tip} = 3.4$ pA reached in the $d \sim 3-10$ nm region. Considering the scheme presented in the inset of Figure 1b, two limiting situations can be envisioned regarding the behavior of the Fc-PEGylated probe within the $d = 10-22$ nm region: For $d_{max}$ values such that $d_{max} > \varepsilon$, the Fc-PEG layer is brought in and out of contact with the substrate, while for $d_{max} < \varepsilon$, the Fc-PEG layer is permanently in contact with the substrate, even though the tip−substrate gap varies periodically in width. Transition between these two limiting situations is reached for $d_{max} = d + A = \varepsilon = 15$ nm. From a simple geometric argument, it can be seen in Figure 1b that this latter equation is valid for $d = 11$ nm, that is, at a point located close to the inflection point of the S-shaped amplitude approach curve (labeled by a star symbol in Figure 1b). As seen in Figure 1c, for this value of *d*, the current is ~3 pA, which is close to the current plateau value of 3.4 pA.

***Zone III:*** ($d \sim 0-3$ nm). From $d = 3$ nm and below, the variation of amplitude with *d* becomes linear and is characterized by a slope $dA/dd = 1$. Such a linear variation is typical of intermittent contact of a hard tip with a hard substrate[45] and is also observed when a bare tip approaches the substrate (green dashed curve in Figure 1b). This behavior demonstrates that the gold surface of the Fc-PEGylated probe is then intermittently touching the surface. As a result, a sharp current increase is observed in the current approach curve. This abrupt current variation is also observed in the approach curve recorded using a bare gold tip (green dashed curve in Figure 1c) and is attributed to tunneling and/or physical contact between the tip and the substrate surfaces. The above analysis of the tapping mode approach curves not only contributes to demon-

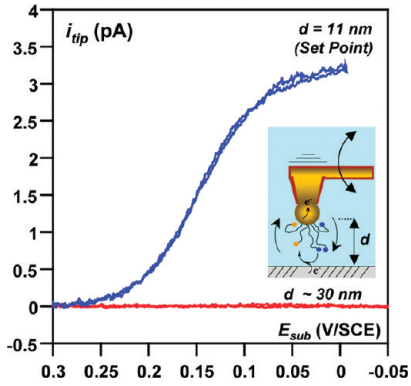


**Figure 2. Cyclic voltammetry at an oscillating Fc-PEGylated probe. The Fc-PEGylated probe is positioned at an average tip-to-substrate distance *d* over the HOPG substrate, set by adjusting the oscillation amplitude imposed by the AFM feedback loop. The substrate potential, $E_{sub}$, is then scanned at 10 mV/s, while the tip−current, $i_{tip}$, is recorded. For $d \sim$ 30 nm, the $i_{tip}$ *vs* $E_{sub}$ voltammogram is "flat". For $d \sim$ 11 nm, the voltammogram is S-shaped, indicating that a faradaic current is then flowing in the Fc-PEGylated probe. Drive frequency = 8.66 kHz, amplitude set point ~ 4 nm. Tip potential: $E_{tip}$ = +0.30 V/SCE; 1 M $NaClO_4$ supporting aqueous electrolyte.**

strate that a molecular layer of Fc-PEG chains is indeed present at the extremity of the tip but also shows that a current can be reliably measured at the oscillating tip for tip−substrate separations close to the size of the $PEG_{3400}$ chain. The nature of the recorded current can be easily established. As explained above, in tapping mode operation, the amplitude is used as the set point of the feedback loop in order to maintain a constant tip−substrate separation. Therefore, setting an amplitude set point of $A \sim 4$ nm allowed an average tip−substrate distance of $d \sim 11$ nm to be permanently maintained by the feedback loop (see Figure 1b). The potential dependence of the recorded tip−current could then be simply acquired by linearly scanning the substrate (or tip) potential. In order to minimize the unwanted current resulting from stray capacitance of the tip, we rather scanned the substrate potential $E_{sub}$ while recording the tip−current $i_{tip}$ ($E_{tip}$ was maintained at +0.30 V/SCE). As seen in Figure 2 when $i_{tip}$ was plotted as a function of $E_{sub}$, a typical S-shaped voltammogram was observed (solid line), which demonstrates the electrochemical (Faradaic) nature of the recorded current. Moreover, the half-wave potential of the voltamogram is ~0.15 V/SCE, which matches the value reported for the standard potential of the Fc heads,[39] thus confirming the specificity of the measured current. Finally, if the amplitude set point was altered to a value very close to, but slightly less than, the free amplitude $A_0$ ($A \sim 0.98 \times A_0 \sim 6.9$ nm), the feedback loop withdrew the tip to $d > 22$ nm, and the then recorded voltammogram was "flat" (see Figure 2). These latter results demonstrate that the recorded current is due to the back and forth motion of the PEG-borne Fc heads, which are alternatively oxidized at the tip and reduced at the substrate (see inset in Figure 2).

The occurrence of such a SECM positive feedback process[1] constitutes the working principle of the Tarm/AFM-SECM microscopy: the Fc heads of the flexible PEG chains borne by the tip are shuttling electrons between the tip and the substrate and are locally sensing the electrochemical reactivity of the substrate. What is also shown here is that such a so-called elastic bounded diffusion SECM positive feedback current[22] can be reliably recorded at an oscillating Fc-PEGylated tip. In that framework, the occurrence of a plateau in the current approach curve for the $d = 3-10$ nm region (Figure 1c) is interpreted as resulting from compression-induced slowing of the PEG chain motion.[22] The possibility of recording an electrochemical current at an oscillating combined AFM-SECM probe has been previously demonstrated in the case of a soluble mediator.[18,25,50] However, in this latter case, the oscillation amplitude, of a few nanometers in magnitude, was very small compared to the much larger diffusion layer of the soluble redox mediator. What is interesting here is that imposing an oscillation to the Fc-PEGylated tip of an amplitude close to the chain size $R_F$ still allows a specific SECM faradaic current to be recorded for average tip−substrate separations ranging from ~5 to 20 nm.

**High-Resolution Topography and Current Imaging Using Tarm/AFM-SECM in Tapping Mode.** The first step to evaluate the imaging capabilities of tapping mode Tarm/AFM-SECM microscopy is to show that the Fc-PEGylated combined probe can be scanned over a planar surface, at a constant tip−substrate distance, while an elastic bounded diffusion SECM positive feedback current is recorded. To this aim, amplitude set point was again set to the value corresponding to the inflection of the amplitude approach curve (*i.e.*, $A = 4$ nm), which kept *d* at a constant value of ~11 nm, and the tip was scanned over a 2 μm × 2 μm area of the HOPG substrate. The images were acquired while keeping the tip potential at a constant value of +0.30 V/SCE and setting the substrate potential at −0.01 V/SCE unless otherwise mentioned.

The topography, applied substrate potential, and recorded tip−current were acquired simultaneously during the scan and are plotted as the corresponding images, respectively, reproduced in parts a, b, and c of Figure 3. Also presented in the lower part of Figure 3 are the cross sections of the corresponding images along the vertical green line shown.

Examination of the topography image (Figure 3a) and corresponding cross section reveals the existence of extremely smooth zones, bordered by step boundaries. The apparent peak-to-peak roughness, as estimated from the cross section shown below the image, is <1 nm. These characteristics are compatible with the known surface topography of HOPG, which consists of atomically flat basal plane areas separated by steps that are the edges of either single monatomic layers (terraces ~0.34 nm in height) or several of these layers stacked. Overall, the topography image acquired with

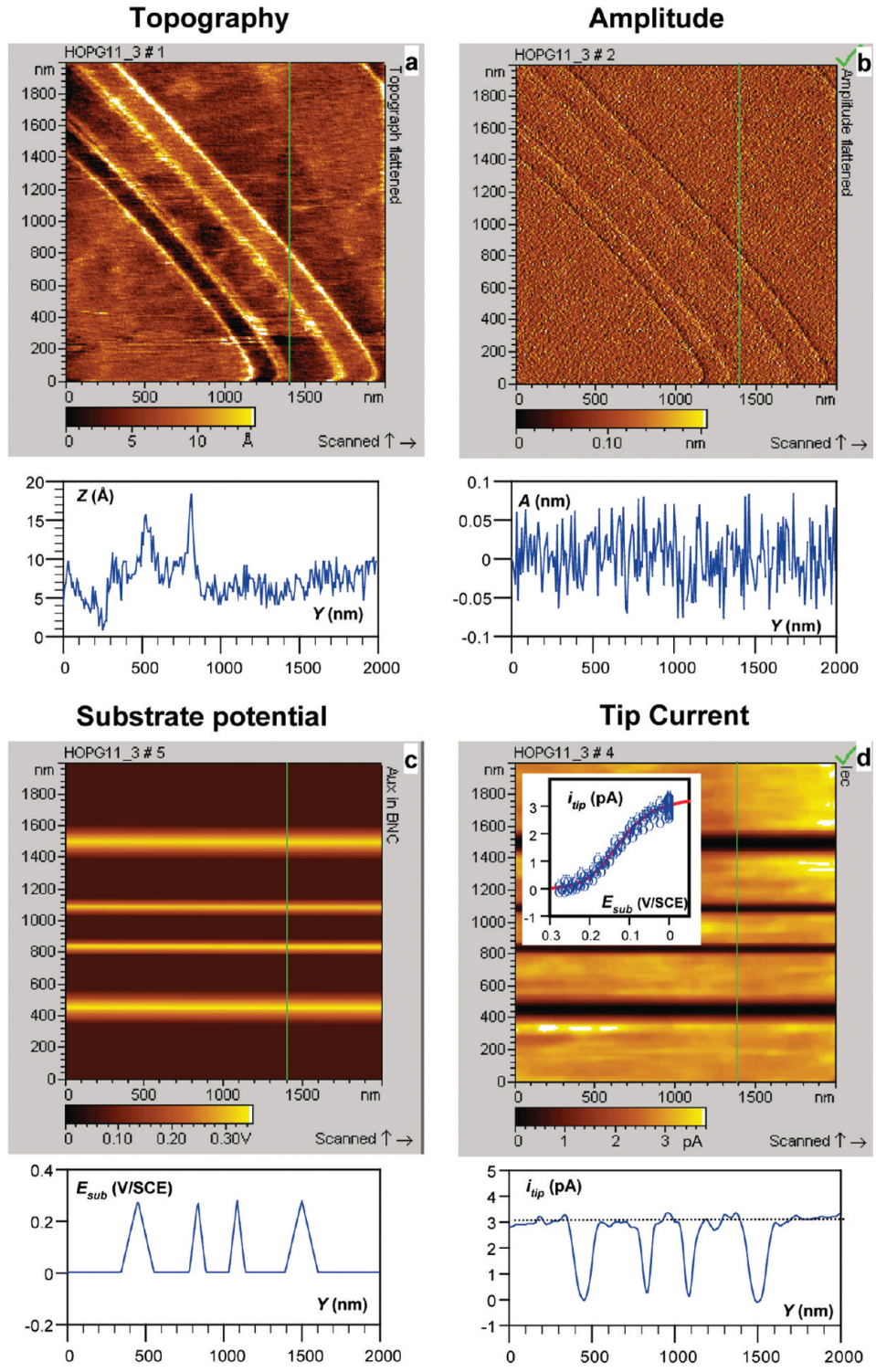


**Figure 3. Tapping mode Tarm/AFM-SECM images acquired by scanning a Fc-PEGylated AFM-SECM probe over a planar HOPG substrate. The simultaneously acquired topography (*Z*), amplitude (*A*), substrate potential ($E_{sub}$), and tip−current ($i_{tip}$) are presented, respectively, in images a, b, c, and d. The cross sections of the images, along the vertical green line shown, are represented in the lower part of the figure, below each corresponding image. During imaging, four substrate potential scans, from $E_{sub} = -0.01$ to $+0.30$ V/SCE, were triggered successively: one at a scan rate of 10 mV/s, followed by two at 5 mV/s, and one at 10 mV/s. The 10 and 5 mV/s scans appear, respectively, as narrow and wide lines in the $E_{sub}$ image reproduced in (c). The inset in (d) is a plot of the $i_{tip}$ data *vs* the $E_{sub}$ data of the cross-section plots: It can be seen that the $i_{tip}$ *vs* $E_{sub}$ data collapse over a unique voltammogram. Drive frequency = 8.66 kHz, amplitude set point ~ 4 nm. Image scan rate = 1 line/s. Tip potential: $E_{tip} = +0.30$ V/SCE; 1 M $NaClO_4$ supporting aqueous electrolyte. The topographic and amplitude images were second order flattened, the $E_{sub}$ and $i_{tip}$ images are raw data.**

our Fc-PEGylated tip in tapping mode shows that a vertical (*Z*) resolution better than 1 nm can be obtained. Similarly, examination of the topographic image reveals that details as small as ~30 nm of the step edges

region visible in the center of the image can be resolved. Considering that large (~500 nm in radius), home-made AFM-SECM probes are used, obtaining such a high-resolution imaging seems surprising. The subnanometric vertical resolution obtained here can be explained by the very good stability of the amplitude feedback mechanism that, as seen in the amplitude image shown in Figure 3b, is able to efficiently maintain the probe oscillation amplitude at a constant value, within less than ±0.1 nm, throughout the image scan. As a result, the feedback loop allows the tip−substrate distance to be kept constant within a few angstroms while the tip closely follows the substrate topography.

The high lateral resolution we obtained may be a benefit of the presence of nanometer-sized corrugations on the gold surface of the probe, with the corrugation located the closest from the surface then playing the role of a very sharp "effective" AFM probe. Going back to analyzing the topography image, one can observe that the boundaries separating the planar regions of the HOPG surface appear as bright lines (see Figure 3a) and, hence, as peaks in the corresponding cross section. Yet, these peaks do not clearly appear in the cross section of the amplitude image, indicating that they cannot be simply attributed to an overshoot of the *Z*-piezo, as sometimes observed when stepped surfaces are imaged by AFM. The observed lines may rather correspond to actual elevated narrow regions, a few tens of nanometer wide and less than 1 nm in height, located at the edges of the steps. Similar so-called distorted step structures have been previously observed on freshly cleaved HOPG by scanning tunneling microscopy (STM).[51]

Turning now to the tip−current image (Figure 3c), we see that it is composed of almost featureless plateaus, corresponding to ~3 pA currents and of horizontal "ditches" at the bottom of which the current intensity is ~0. The plateaus correspond to areas where the tip and substrate potentials were kept at $E_{tip}$ +0.30 V/SCE and $E_{sub}$ = −0.01 V/SCE. The current within these areas is observed to be almost constant, with less than 0.3 pA fluctuations, over large scan areas encompassing "planar" and edge features, as identified from the topography image. In order to ascertain the origin of the current recorded during the image scan, the substrate potential was periodically scanned from −0.01 V up to +0.30 V/SCE and back to −0.01 V. Two potential scans were triggered at a scan rate of 10 mV/s and two at a scan rate of 5 mV/s. The actual substrate potential, $E_{sub}$, was acquired during imaging and is presented in Figure 3b as an "$E_{sub}$ image". In this latter image, the potential scans appear as bright lines, with the 10 and 5 mV/s scans appearing, respectively, as narrow and wide lines. Examining the $i_{tip}$ image, and its cross section, we see that in response to the potential scan the current varies smoothly from a maximum value of 3 pA, measured for $E_{sub}$ = −0.01 V and down to 0 pA for $E_{sub}$ = $E_{tip}$ = 0.30 V. This $i_{tip}$ *versus* $E_{sub}$ variation is seen more clearly if the current recorded along any vertical cross section of the $i_{tip}$ image is plotted as a function of the corresponding cross section of the $E_{sub}$ image, as shown in the inset of Figure 3c. It can be seen that the $i_{tip}$ *versus* $E_{sub}$ data then collapse into a single voltammogram, similar to the one shown in Figure 2. Importantly, this means that the same voltammogram is obtained from the data acquired at potential scan rates of 5 and 10 mV/s, which demonstrates that no time-dependent phenomenon, such as capacitive coupling between the tip and substrate, contributes to the current signal. Moreover, the half-wave potential of the reconstructed voltammogram, of ~0.13 V/SCE, is close to the standard potential of the Fc head (0.15 V/SCE), indicating that the recorded current corresponds solely to the electrochemistry of the Fc heads. This result confirms the fact that the current recorded during imaging is indeed due to the tip−substrate motion of the Fc heads borne by the tip and associated electron transfers, as depicted in Figure 2.

We thus demonstrated that the Fc heads borne by the oscillating tips are able to locally probe the electrochemical reactivity of the substrate, which was here made artificially heterogeneous by modulating the substrate potential. This result is conceptually transposable to the case of a composite surface probed by Tarm/AFM-SECM, where the local electrochemical reactivity will be modulated by the presence, and/or the specific activity, of nanometer-sized redox sites. Importantly, as can be seen by examining Figure 3a,e, scanning the substrate potential during imaging did not affect the measured topography nor amplitude, thus showing that the tip−substrate interactions responsible for the damping of the tip oscillation do not depend on the substrate potential. We verified that the topography image was also tip potential independent. This ability of scanning (or changing) the tip or substrate potential without affecting the topography image is expected to be of utmost importance for Tarm/AFM-SECM imaging since it will allow one to locate active sites on surfaces from the topography image while simultaneously ascertaining that the contrast mechanism of the current image is of electrochemical origin (*i.e.*, that the current image solely reflects the electrochemical reactivity of the active sites).

**Probing the Electrochemical Reactivity of a Composite Substrate by Tapping Mode Tarm/AFM-SECM.** In order to demonstrate that isolated electroactive sites present on a substrate surface can be discriminated by Tarm/AFM-SECM, we imaged a model composite surface (*i.e.*, a surface presenting well-defined electrochemically active and inactive areas). This model substrate was a micropatterned $SiO_2$ surface bearing an array of band electrodes, 500 nm in width and 25 nm in height, made of evaporated gold. Even though this substrate was well-

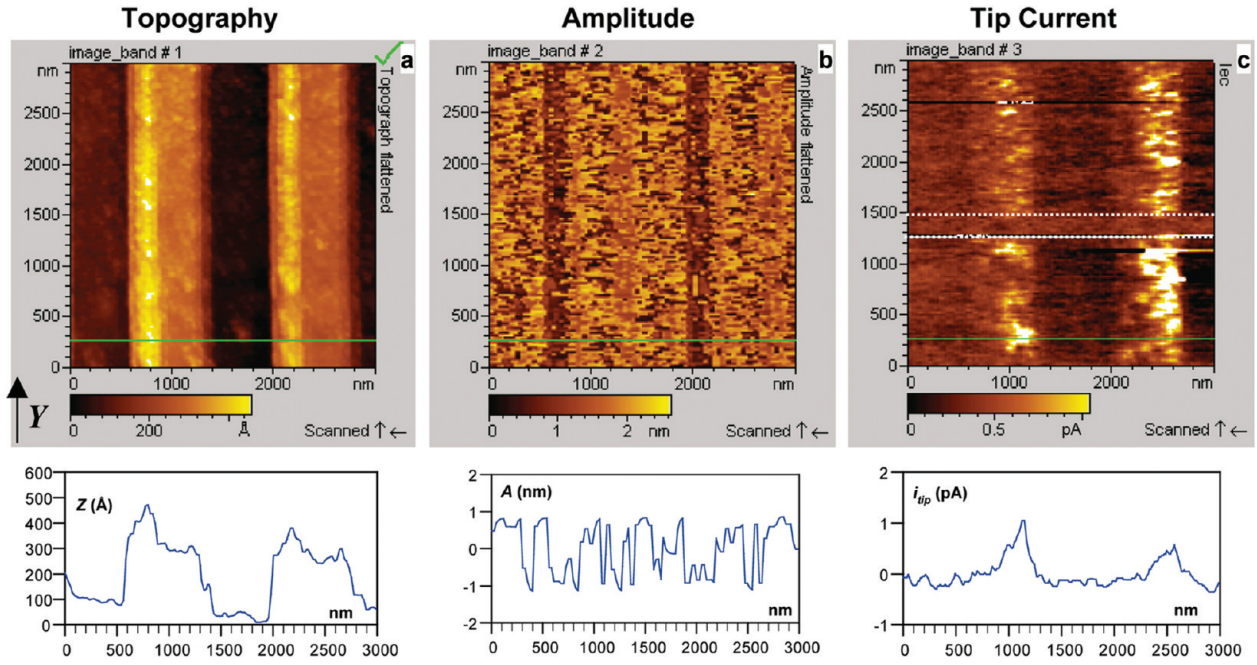


**Figure 4. Tapping mode Tarm/AFM-SECM imaging of a patterned substrate, consisting of 500 nm wide, ~25 nm high gold band electrodes deposited on $SiO_2$. The simultaneously acquired topography (*Z*), amplitude (*A*), and tip−current ($i_{tip}$) are presented, respectively, in images a, b, and c. The cross sections of the images, along the short green line shown, are represented in the lower part of the figure, below each corresponding image. The tip potential was set to $E_{tip}$ = +0.25 V/SCE. The potential of the band electrodes was set to $E_{sub}$ = −0.01 V/SCE for the regions of the image located above and below the pair of dotted white lines shown in c. Between these lines, the substrate potential was raised to +0.30 V/SCE. Drive frequency = 4.28 kHz, amplitude set point 0.24 V (free amplitude 0.27 V), image scan rate = 0.1 Hz. The topography and amplitude images were first order flattened, and the current image is raw data. See Supporting Information for the retrace images.**

defined geometrically, it had a major disadvantage: the gold surface of the band electrodes was observed to be actually quite "rough", displaying sharp ~10−20 nm high corrugations especially at the band edges (as seen from the AFM image provided in Supporting Information). These corrugations resulted in the occurrence of numerous tip−substrate short-circuits during Tarm/AFM-SECM imaging of the patterned surface. In order to minimize this phenomenon, the image scan rate had to be set to a very low value (0.1 Hz). For the same reason, the amplitude set point had to be set to a value very close to the free oscillation amplitude of the probe (~10% damping). The band electrodes were interconnected, and their potential, $E_{sub}$, was initially set to −0.01 V/SCE. The tip potential was set to $E_{tip}$ = +0.25 V/SCE. Topography, amplitude, and current signals were acquired simultaneously, and the corresponding images are presented in Figure 4.

The band electrodes can be clearly distinguished from the topography image, and their average height, *h* ~ 30 nm, is close to their nominal height. Their apparent width is ~750 nm, which is larger than their actual width. As detailed in Supporting Information, this is due to the well-known tip convolution effect: the apparent width of a band electrode imaged using a spherical tip of radius $R_{tip}$ is expected to be overestimated by ~2 × $(2hR_{tip})^{1/2}$, that is, by ~300 nm, taking $R_{tip}$ ~ 500 nm. One can also observe in the topography image the presence of ~10−20 nm high ridges near the left edge of the bands. These ridges contribute the most to the overall roughness of the band electrodes and are a down side of the process used to fabricate the patterned surface (see Methods section).

The band electrodes also appear very clearly in the upper part of the current image, for which the substrate potential was constant and set to $E_{sub}$ = −0.01 V/SCE. This part of the image corresponds to the beginning of the scan since the image was acquired from top to bottom. The relative low current measured (<1 pA) arises from the fact that, as explained above, imaging had to be carried out under a weak damping regime, which in turn means a large average tip−substrate distance and hence a low current (see Figure 1). In the central part of the image, delimited by the two white dotted lines visible in Figure 4c, the substrate potential was set to + 0.3 V/SCE during the acquisition of the image (see Supporting Information). At such a positive potential, reduction of the Fc head at the substrate cannot occur. As a result, one can see that the contrast of the current image is totally lost. When $E_{sub}$ was set back to its initial value of −0.01 V/SCE, the current contrast was observed to be fully restored, as seen in the bottom part of the current image. This result indicates that the current recorded when the tip is scanned over the band electrodes is due to the electrochemistry of

the Fc heads. One can also see from Figure 4c that, no matter the value of $E_{sub}$, no current variation (and hence no contrast) is observed over the insulating regions of the composite substrate. All of the above is a clear demonstration that Tarm/AFM-SECM does allow the activity of sub-micrometer-sized electrochemical sites, isolated on an insulating surface, to be probed.

Examining further the current image, one can see that the current is not constant over the whole surface of the band electrodes. This probably is an artifact due to the fact that the gold surface of the band electrodes was actually quite "rough", as discussed above. This rough topography may not be closely followed by the quite large tip, resulting in a varying tip−substrate distance as sensed by the chains generating the current and, hence, to a current signal partly convoluted to topography. A way around this problem would have been to use smaller-sized tips. In any case, one can estimate that, for Tarm/AFM-SECM to be used reliably, the roughness of the sample has to be kept below the chain size (*i.e.*, not exceeding ~10 nm). Substrate roughness limitations are common to local probe techniques.

We then used Tarm/AFM-SECM to probe the electrochemical activity of HOPG, which is an ideal substrate for our study, not only because it is flat but also because this material reputedly displays an electrochemical activity which is heterogeneous at the nanoscale (*i.e.*, step edges are more reactive than planar sites).[52]

**Probing the Nanostructured Electrochemical Reactivity of HOPG by Tapping Mode Tarm/AFM-SECM.** Upon examining the Tarm/AFM-SECM images of a HOPG surface presented in Figure 3, one can notice that the edges of the basal planes, which can be seen in the topography image, cannot be distinguished in the feedback current image. Since it is well-known that the heterogeneous electron transfer rate on HOPG is markedly faster at step edges than at basal planes,[52] one might have expected a larger electrochemical current at step edge sites. However, one should recall that these images were acquired with $E_{sub}$ set to a high enough value for the current to be solely controlled by chain dynamics, that is, to be independent of the charge transfer rate at the substrate (see above). In an attempt to discriminate the electron transfer rate at the edge and basal planes of HOPG, the surface was imaged in tapping mode Tarm/AFM-SECM microscopy at a more anodic $E_{sub}$ value of +0.20 V/SCE, corresponding to the foot of the voltammogram presented in Figure 2. At this potential, the rate of heterogeneous electron transfer at the HOPG substrate may participate in the kinetic control of the faradaic current. Figure 5, panel A, presents the corresponding simultaneously acquired topography, amplitude, and feedback current images. One can see that the characteristic features of the HOPG surface are very clearly resolved in the topographic image presented in Figure 5a, panel A. In particular, long lines, corresponding to the edges of graphite planes, are clearly visible. Although the current image is quite noisy, due to the low intensity of the current recorded at $E_{sub} = +0.2$ V/SCE (~0.5 pA), one can see two faint, yet very discernible lines across the current image, which can be associated with the two lines of edge sites visible in the center of the topographic image. More quantitatively, examination of the cross sections of the images, cut along the short green line shown, reveals that when the Fc-PEGylated probe passed above a step separating two graphite planes the current increased by ~0.3 pA (see lower part of Figure 5, panel A).

Importantly, when the same area of the sample is subsequently scanned with the substrate potential set to $E_{sub} = +0.3$ V/SCE, that is, to a potential such that reduction of the oxidized Fc heads cannot occur, the lines disappear from the current image while the topography and amplitude images are unchanged (see Figure 5, panel B). This latter result allows one to exclude that the bright lines observed in the current image shown in Figure 5c, panel A, are artifacts induced by the *Z* motion of the tip, or resulting from a cross-talk between the topography and the current recording channels, as often feared when combined AFM techniques are used. At the opposite, the observed $E_{sub}$ dependence of the current image indicates that this latter image does reflect the local electrochemical reactivity of the substrate. We thus ascribe the lines visible in the current image shown in Figure 5, panel A, to an enhanced electron transfer rate at step edges with respect to the basal plane of HOPG. However, we note that not all of the step edges visible in the topography image give rise to a detectable increase in tip−current. For example, the steps observed in the upper right part of the topographic image in Figure 5a, panel A, are barely detected in the corresponding current image. The physical reason behind the dissimilar behavior of the two series of steps observed is not clear at this stage. Yet, incidentally, this result provides evidence that the current and topography measurements reported here are fully decoupled since features similar in size (here step height) but differing solely by their electrochemical behavior can be discriminated.

Probing locally the heterogeneity of the electrochemical reactivity of HOPG by SECM, as is achieved here, is quite of a challenge that, to the best of our knowledge, has only been met once, in a recent paper by Frederix *et al.*[53] These authors, using integrated microfabricated AFM-SECM nanoprobes and a soluble mediator, also recorded current "peaks" corresponding to the location of step edges of

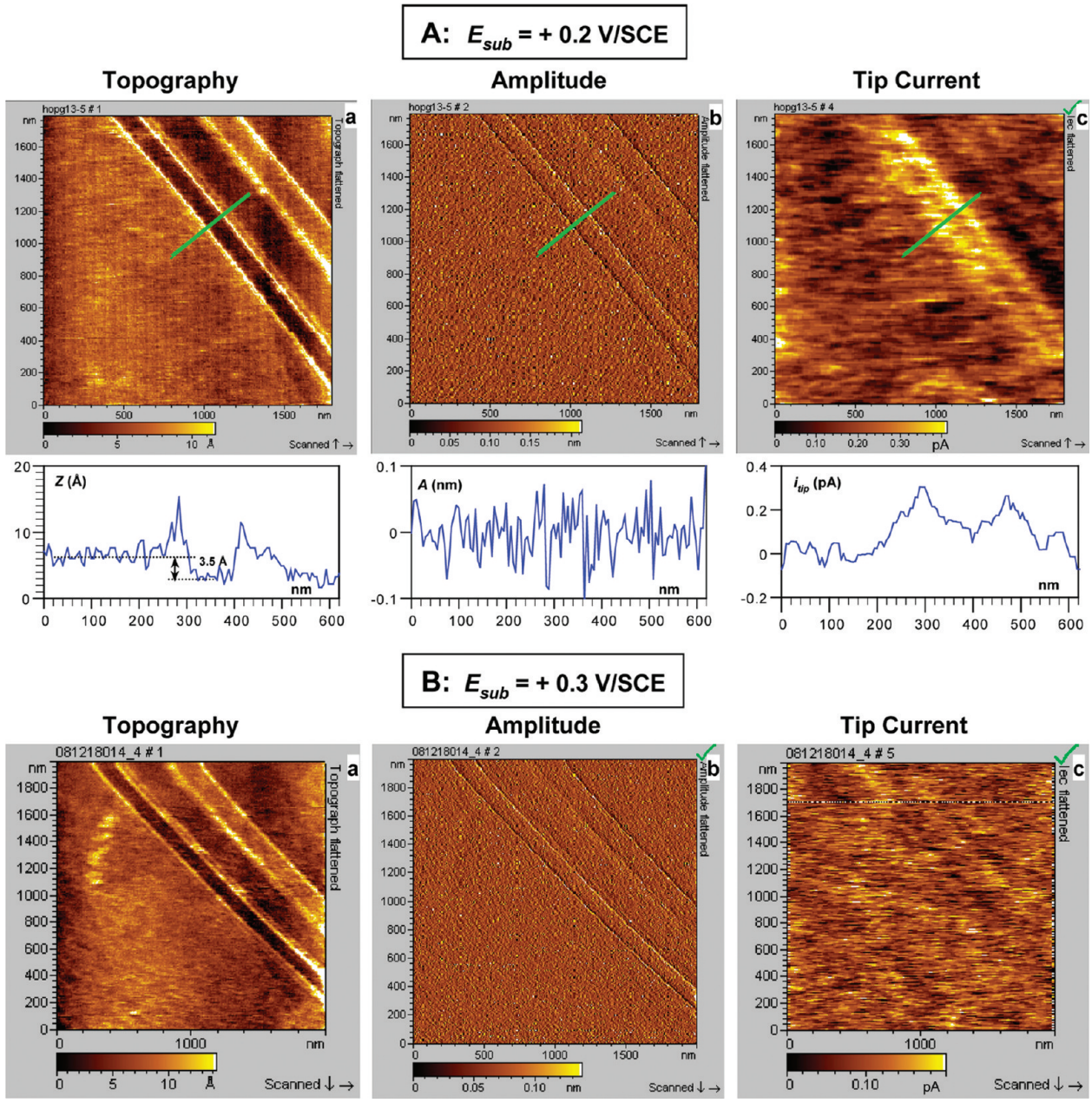


**Figure 5. Tapping mode Tarm/AFM-SECM imaging of a HOPG substrate: discriminating the electron transfer rate of the Fc heads at edge sites and at the basal planes of the HOPG surface. The simultaneously acquired topography (*Z*), amplitude (*A*), and tip−current ($i_{tip}$) are presented, respectively, in images a, b, and c. The cross sections of the images, along the short green line shown, are represented in the lower part of the figure, below each corresponding image. The tip potential was set to $E_{tip}$ = +0.30 V/SCE. Panel A: Substrate potential was set to $E_{sub}$ = +0.20 V/SCE. At this potential, reduction of the oxidized Fc heads is expected to be slow. The edge sites are clearly resolved in the topography image and for some of them also in the current image (see text). Panel B: Same area of the HOPG substrate was subsequently imaged with $E_{sub}$ set to + 0.30 V/SCE. At this potential, reduction of the oxidized Fc heads does not occur. As a result, the current contrast vanishes. Drive frequency = 8.66 kHz, amplitude set point ~ 4 nm; 1 M $NaClO_4$ supporting aqueous electrolyte. Image scan rate 1 line/s. The topography and amplitude images were second order flattened, and the current image was first order flattened. See Supporting Information for raw data.**

HOPG. In agreement with our results, they did not observe these peaks for all of the step edges visible in their topographic images.

The data collected here can be used for semiquantitative assessment of the rate of heterogeneous electron transfer of the Fc heads at basal planes and at step sites of HOPG. The $i_{tip}$ *versus* $E_{sub}$ voltammograms (CVs) recorded with the tip positioned above clearly identified that basal planes are similar to the CV shown in Figure 2. Their analysis indicates a quasi-reversible behavior of the Fc heads at the HOPG surface (see Supporting Information). This observation simply means that the rate of mass transfer of the Fc heads and the rate of electron transfer at the surface are comparable in magnitude. In our previous paper, we estimated that the

mass transfer rate of the heads of Fc-$PEG_{3400}$ chains attached to a steady (*i.e.*, non-oscillating) tip was on the order of ~0.05 cm/s.[34] The heterogeneous electron transfer rate constant of the Fc heads at basal planes of HOPG is thus expected to be comparable to this latter value, assuming that the contribution of tip oscillation to chain dynamics can be neglected. Such an assumption appears legitimate because, for a typical oscillation frequency of ~ 10 kHz, the probe motion is in the $10^{-4}$ s time range, while Fc-PEG chain dynamics is at least 10 times faster.[34]

Qualitatively speaking, we therefore observed that basal planes of HOPG display a relatively high electrochemical reactivity with respect to the Fc heads. This result is in agreement with a recent study which, by making use of a scanning micropipet contact method, showed that basal plane HOPG was highly active toward the redox reaction of a ferrocene derivative, trimethylamminomethyl ferrocene.[54]

As far as the rate of electron transfer at step edges of HOPG is concerned, the ~0.3 pA increase in current we typically recorded when the tip was scanned over a step is compatible with the electron transfer rate at the steps becoming much faster than mass transfer of the Fc heads. In the present case, the electron transfer rate at step sites needs to be at least ~4 times faster than at basal plane HOPG for this condition to be fulfilled (see Supporting Information).

Beyond mere characterization of the heterogeneous reactivity of the HOPG surface, the results we report here demonstrate the ability of tapping mode Tarm/AFM-SECM microscopy to map the reactivity of nanometer-sized active sites on a substrate surface (here HOPG step sites). Moreover, in the context of the present paper, imaging HOPG also allows the lateral resolution of Tarm/AFM-SECM microscopy to be experimentally determined. If one neglects the observed finite width of the edge region of the HOPG steps, and thus considers that these steps are perfectly sharp, the width of the peak-shaped current variation recorded when the probe passes over a step then reflects the size of the interaction area between the Fc-PEG chains and the substrate. From the current cross-section data presented in Figure 5, panel A, one can measure that the width at midheight of the current peaks is ~100 nm, indicating that the Fc-PEG chains actually probe a disk-shaped area which is ~50 nm in radius. This latter value can thus be taken as a lower estimate of the resolution of the Tarm/AFM-SECM microscopy attained here. For a tip radius of ~500 nm and a typical chain coverage of ~$10^{-11}$ mol/$cm^2$,[34] it can thus be estimated, from a simple calculation, that ~450 Fc-PEG chains, located at the tip extremity, are actually contacting (sensing) the substrate surface. The ability to detect such a relatively low number of chains is due to the fact that redox cycling of the Fc heads between the tip and substrate constitutes in itself an amplification mechanism that, for other systems, has been reported to even allow the detection of single molecules.[55−57] These results also illustrate that, thanks to the nanometer size of the PEG chains, the tip−substrate interaction area is reduced to a fraction of the size of the supporting spherical probe. It is thus expected that the electrochemical resolution of Tarm/AFM-SECM microscopy can be improved down to the limit given by the effective chain size (~10 nm) by using AFM-SECM probes ~100 nm in radius such as the ones we reported previously.[20] An attractive feature of Tarm/AFM-SECM is that the overall redox/chemical environment of the sample is not perturbed since no artificial soluble mediator needs to be added to the solution, which may be a benefit for studying fragile systems. This advantage may be partly counter-balanced by the workload required to synthesize linear polymer chains to attach the mediator to the probe. Yet the versatility of the PEG chain functionalization method we described previously,[34] and used here, should allow the preparation of heterofunctionalized PEG chains that can bear a large variety of redox mediators and anchoring groups for tip attachment.

## CONCLUSION

In conclusion, we have developed a new type of high-resolution AFM-SECM microscopy, we label Tarm (for tip-attached redox mediator)/AFM-SECM, where the redox mediator is tethered to the AFM-SECM probe *via* nanometer long, flexible PEG chains. We have demonstrated that the tip-attached ferrocene-labeled PEG chains effectively shuttle electrons between the tip and substrate, thus acting as molecular sensors probing the local electrochemical reactivity of a planar substrate. Moreover, we have shown that Fc-PEGylated AFM-SECM probes can be used for tapping mode imaging, allowing simultaneous recording of electrochemical feedback current and of topography with a vertical and a lateral resolution in the nanometer range. By imaging a model HOPG substrate, we demonstrated that Tarm/AFM-SECM microscopy can be used to probe the reactivity of nanometer-sized active sites on surfaces. Tarm/AFM-SECM could ultimately enable functional imaging of individual redox enzyme molecules, providing that the ~fA response from a single enzyme molecule can be measured.[32] In its tapping mode, Tarm/AFM-SECM microscopy can be viewed as the electrochemical equivalent of TREC (*t*opography and *rec*ognition) microscopy,[58,59] where biomolecules capable of molecular recognition (IgGs, avidin, aptamers, *etc.*) are attached to the extremity of an AFM tip *via* a flexible polymer tether. Using these functional-

ized tips, specific host−guest interactions can be detected while high-resolution topography of the surface is acquired. Similarly, it is expected that tapping mode Tarm/AFM-SECM microscopy will allow isolated surface-bound redox enzyme molecules to be located from topographic images while their individual catalytic activity will be simultaneously probed. More generally, Tarm/AFM-SECM microscopy can be viewed as a new scanning probe tool for nanochemistry since it allows a redox reactant to be delivered in a controlled way at specific nanometer-sized locations on surfaces.

## METHODS

**Experimental Procedures.** ***Preparation of the [Fc-PEG$_{3400}$-S]$_2$ Disulfide and Materials.*** The linear [Fc-PEG$_{3400}$-S]$_2$−disulfide molecules (~79 monomer units per chain) were synthesized as described previously.[34,38] Sodium perchlorate ($NaClO_4$) monohydrate was purchased from Merck. Other commercial chemicals were reagent grade or better quality and used as received. All aqueous solutions were made with Milli-Q purified water (Millipore). All solvents used for PEG grafting of AFM-SECM probes as well as AFM-SECM experiments were filtered before use on a 0.22 μm nylon Cameo filter.

***Preparation of the HOPG Substrate Surface.*** The HOPG surface was from Goodfellow and cleaved using scotch tape before each experiment. HOPG was chosen for the tapping mode operation using Fc-PEGylated probes and ensuing imaging experiments, due to its naturally nanostructured topography, consisting of easily identifiable terraces, edges, and defects.

***Fabrication of the Patterned Substrate.*** The patterned surface, bearing an array of band electrodes, was fabricated using electron-beam lithography technique and a single layer negative tone lift-off resist process, which was adapted from previous work.[60] First, a silicon substrate was covered by a nonconductive layer made of 1 μm thick silicon dioxide ($SiO_2$). This film was obtained by plasma-enhanced chemical vapor deposition (PECVD). The metallic gratings are defined by EBL (VISTEC EBPG5000plus Gaussian electron beam lithography system operating at 100 kV) on a 250 nm layer of a commercially available negative-tone resist (ma-N 2403, Micro-Resist) spin-coated on the $SiO_2$ layer. After resist development in a MIF 726 developer, a titanium/gold (5 nm/20 nm) layer was deposited by electron-beam-assisted evaporation and lifted-off in acetone. The thin titanium layer was used to improve the gold adhesion onto the $SiO_2$ layer.

***Measurement of the Spring Constants of the Tips. Estimation of the Spherical Microelectrode Probe Size.*** The spring constant of the combined probe, $k_{probe}$, was estimated from the measured dimensions of the flattened part of the wire-based probe that acted as a rectangular cantilever, using the formula $k_{probe} = Ewt^3/4l^3$, where $w$, $t$, and $l$ are, respectively, for the cantilever width, thickness, and length and $E$ is the elastic modulus of gold (~80 GPa). The spring constant of each probe was also measured using a reference cantilever pushing against the flexible arm of the combined AFM-SECM probe; both methods yielded similar spring constant values in the ~1 − 2 N/m range (see ref 34 for details). The size of the spherical gold AFM-SECM probes was either simply estimated from optical microscopy or measured using scanning electron microscopy after they were used in AFM-SECM experiments. In some cases, the spherical extremity of the probe was "imaged" using AFM, as detailed in Supporting Information. This latter approach also allowed the nanometer-sized roughness of the probe surface to be estimated (see Supporting Information).

***AFM-SECM Experiments.*** The AFM/SECM experiments were performed with a Molecular Imaging PICOSPM AFM microscope (Scientec, France), which was modified and operated as previously described.[21] A home-made bipotentiostat enabled us to independently apply the electrochemical tip and substrate potentials with respect to a reference electrode (a platinum wire/polypyrrole quasi-reference electrode; see below). The tip and substrate currents were measured by the high (100 pA/V) and low (20 μA/V) gain current measuring circuits of the bipotentiostat. The bandwidth of the bipotentiostat was estimated to be in the ~10−20 kHz range. The tip−current signal was filtered using an adjustable low-pass analogue filter. The lowest cutoff frequency used was 10 Hz. We made sure that the frequency chosen for the filter was always high enough not to distort the recorded current images or current approach curves. The substrate potential was generated by a PAR 175 programmer, and the substrate current data were acquired on a digital oscilloscope. The Molecular Imaging PICOSCAN controller was used to generate the tip potential and to acquire the tip−current data. Experiments were carried out *in situ* in a fluid cell containing an aqueous 1 M $NaClO_4$ electrolyte solution. A positive potential was preferentially applied to the tip in order to prevent any cathodic stripping of the Fc-PEG chains from the tip, during the time course of the hour-long experiments. However, we verified that swapping the tip and substrate potential solely resulted in changing the sign of the recorded current and not the shape nor the intensity of the approach curves. This indicates that the Fc heads are stable in both their oxidized ($Fc^+$) and their reduced states (Fc), in the 1 M $NaClO_4$ medium used. The tip and substrate potentials were measured *in situ* with respect to a platinum wire/polypyrrole quasi-reference electrode (Pt/PPy) that was fabricated according to a procedure adapted from the literature.[61] Briefly, a polypyrrole film was electrochemically deposited on a platinum wire by cyclic voltammetry (50 cycles between −0.6 and 1.4 V *vs* SCE) in an acetonitrile solution containing 0.01 M pyrrole and 0.1 M $Bu_4NPF_6$. The final cycle was stopped at 0.65 V/SCE for 30 s in order to partially oxidize the film. The platinum/polypyrrole quasi-reference electrode was rinsed with acetone and soaked in pure acetonitrile for 1 h. After 30 min immersion in 1 M $NaClO_4$, to exchange the $PF_6^-$ counterion for $ClO_4^-$, the open-circuit potential (OCP) was measured. The Pt/PPy reference showed a stable OCP of + 0.165 V/SCE in 1 M $NaClO_4$. The quasi-reference electrode was stored in 0.1 M $NaClO_4$ and could be used for over 1 week. The tip−current approach curves and images were corrected from a small leakage current of ≤1 pA, which resulted from the imperfect insulation of the tip and of the connecting wires. This current is nonspecific and independent of the tip−substrate distance and of the tip and substrate potential. Dozens of approach curves could be recorded with each of the ~10 Fc-PEGylated probes we successfully fabricated, demonstrating the stability of the Fc-PEG layer. In a typical experiment, the tip and substrate potentials were $E_{tip} = +0.30$ V/SCE and $E_{sub} \leq -0.01$ V/SCE.

***Tapping Mode Operation: Conversion of the Raw Amplitude versus Piezo Elongation Data into Amplitude versus Tip−Substrate Distance Curves.*** Multiplying the raw amplitude data (in volts), as acquired by the AFM controller, by the gains indicated by the manufacturer, and taking into account the measured sensitivity factor of the PSD, allowed the tip oscillation amplitude $A$ (in nanometers) to be obtained. The thus found volt-to-nanometer conversion factor was also used to set the scale of the amplitude images. $Z_0$, the piezo elongation corresponding to hard contact between the probe and the HOPG substrate, was taken as the point on the current approach curve where the tip−current raised abruptly. Knowing $Z_0$ allowed the time-averaged tip−substrate separation $d$ to be derived from the piezo elongation, as described in the text. The consistency of the $A$ and $d$ determination from raw data was ascertained by the observation of a slope $dA/dd$ such that $dA/dd = 1$ for $d \rightarrow 0$ because this behavior is expected for a hard tip contacting intermittently a hard substrate.[44]

*Supporting Information Available:* Acoustic excitation spectrum of the Fc-PEGylated probe used for Tarm/AFM-SECM imaging. Characterization of the patterned gold bands/$SiO_2$ surface by tapping mode AFM. Trace and retrace Tarm/AFM-SECM images of the patterned surface. Raw current images corresponding to Figure 5. Scanning electron microscopy and AFM images

of home-made AFM-SECM used in this work. Geometrical evaluation of the tip convolution effect when imaging a sharp step with a spherical tip. Estimation of the heterogeneous electron transfer rate constant for the Fc heads at basal planes and at step sites of HOPG from cyclic voltametry and current image data. This material is available free of charge *via* the Internet at http://pubs.acs.org.

## REFERENCES AND NOTES


1. *Scanning Electrochemical Microscopy*; Bard, A. J., Mirkin, M. V., Eds.; Marcel Dekker: New York, 2001; pp 1−15.
2. Sun, P.; Laforge, F. O.; Mirkin, M. V. Scanning Electrochemical Microscopy in the 21st Century. *Phys. Chem. Chem. Phys.* **2007**, *9*, 802–823.
3. Wittstock, G.; Burchardt, M.; Pust, S. E.; Shen, Y.; Zhao, C. Scanning Electrochemical Microscopy for Direct Imaging of Reaction Rates. *Angew. Chem., Int. Ed.* **2007**, *46*, 1584–1617.
4. Borgwarth, K.; Heinze, J. In *Scanning Electrochemical Microscopy*; Bard, A. J., Mirkin, M. V., Eds. Marcel Dekker: New York, 2001; pp 201−238.
5. Wipf, D. O.; Bard, A. J. Scanning Electrochemical Microscopy. 10. High Resolution Imaging of Active Sites on an Electrode Surface. *J. Electrochem. Soc.* **1991**, *138*, L4–L6.
6. Engstrom, R. C.; Small, B.; Kattan, L. Observation of Microscopically Local Electron-Transfer Kinetics with Scanning Electrochemical Microscopy. *Anal. Chem.* **1992**, *64*, 241–244.
7. Lee, J.; Ye, H.; Pan, S.; Bard, A. J. Screening of Photocatalysts by Scanning Electrochemical Microscopy. *Anal. Chem.* **2008**, *80*, 7445–7450.
8. Bard, A. J.; Mirkin, M. V.; Unwin, P. R.; Wipf, D. O. Scanning Electrochemical Microscopy. 12. Theory and Experiment of the Feedback Mode with Finite Heterogeneous Electron-Transfer Kinetics and Arbitrary Substrate Size. *J. Phys. Chem.* **1992**, *96*, 1861–1868.
9. Borgwarth, K.; Heinze, J. Increasing the Resolution of the Scanning Electrochemical Microscope Using a Chemical Lens: Application to Silver Deposition. *J. Electrochem. Soc.* **1999**, *146*, 3285–3289.
10. Ufheil, J.; Hess, C.; Borgwarth, K.; Heinze, J. Nanostructuring and Nanoanalysis by Scanning Electrochemical Microscopy (SECM). *Phys. Chem. Chem. Phys.* **2005**, *7*, 3185–3190.
11. Etienne, M.; Anderson, E. C.; Evans, S. R.; Schuhmann, W.; Fritsch, I. Feedback-Independent Pt Nanoelectrodes for Shear Force-Based Constant-Distance Mode Scanning Electrochemical Microscopy. *Anal. Chem.* **2006**, *78*, 7317–7324.
12. Sun, P.; Mirkin, M. V. Kinetics of Electron-Transfer Reactions at Nanoelectrodes. *Anal. Chem.* **2006**, *78*, 6526–6534, and references cited therein.
13. Tel-Vered, R.; Walsh, D. A.; Mehrgardi, M. A.; Bard, A. J. Carbon Nanofiber Electrodes and Controlled Nanogaps for Scanning Electrochemical Microscopy Experiments. *Anal. Chem.* **2006**, *78*, 6959–6966.
14. Watkins, J. J.; Chen, J.; White, H. S.; Abruña, H. D.; Maisonhaute, E.; Amatore, C. Detection and Electron-Transfer Rate Measurements Using Platinum Electrodes of Nanometer Dimensions. *Anal. Chem.* **2003**, *75*, 3962–3971.
15. Macpherson, J. V.; Unwin, P. R.; Hillier, A. C.; Bard, A. J. *In-Situ* Imaging of Ionic Crystal Dissolution Using an Integrated Electrochemical/AFM Probe. *J. Am. Chem. Soc.* **1996**, *118*, 6445–6452.
16. Macpherson, J. V.; Unwin, P. R. Combined Scanning Electrochemical-Atomic Force Microscopy. *Anal. Chem.* **2000**, *72*, 276–285.
17. Macpherson, J. V.; Unwin, P. R. Non-Contact Electrochemical Imaging with Combined Scanning Electrochemical-Atomic Force Microscopy. *Anal. Chem.* **2001**, *73*, 550–557.
18. Burt, D. P.; Wilson, N. R.; Weaver, J. M. R.; Dobson, P. S.; Macpherson, J. V. Nanowire Probes for High Resolution Combined Scanning Electrochemical Microscopy-Atomic Force Microscopy. *Nano Lett.* **2005**, *5*, 639–643.
19. Kranz, C.; Friedbacher, G.; Mizaikoff, B.; Lugstein, A.; Smoliner, J.; Bertagnolli, E. Integrating an Ultramicroelectrode in an AFM Cantilever. Combined Technology for Enhanced Information. *Anal. Chem.* **2001**, *73*, 2491–2500.
20. Abbou, J.; Demaille, C.; Druet, M.; Moiroux, J. Fabrication of Submicrometer-Sized Gold Electrodes of Controlled Geometry for Scanning Electrochemical-Atomic Force Microscopy. *Anal. Chem.* **2002**, *74*, 6355–6363.
21. Abbou, J.; Anne, A.; Demaille, C. Probing the Structure and Dynamics of End-Grafted Flexible Polymer Chain Layers by Combined Atomic Force-Electrochemical Microscopy. Cyclic Voltammetry within Nanometer-Thick Macromolecular Poly(ethylene glycol) Layers. *J. Am. Chem. Soc.* **2004**, *126*, 10095–10108.
22. Abbou, J.; Anne, A.; Demaille, C. Accessing the Dynamics of End-Grafted Flexible Polymer Chains by Atomic Force-Electrochemical Microscopy. Theoretical Modeling of the Approach Curves by the Elastic Bounded Diffusion Model and Monte Carlo Simulations. Evidence for Compression-Induced Lateral Chain Escape. *J. Phys. Chem. B* **2006**, *110*, 22664–22675.
23. Frederix, P. L. T. M.; Gullo, M. R.; Akiyama, T.; Tonin, A.; de Rooij, N. F.; Staufer, U.; Engel, A. Assessment of Insulated Conductive Cantilevers for Biology and Electrochemistry. *Nanotechnology* **2005**, *16*, 997–1005.
24. Gullo, M. R.; Frederix, P. L. T. M.; Akiyama, T.; Engel, A.; de Rooij, N. F.; Staufer, U. Characterization of Microfabricated Probes for Combined Atomic Force and High-Resolution Scanning Electrochemical Microscopy. *Anal. Chem.* **2006**, *78*, 5436–5442.
25. Hirata, Y.; Yabuki, S.; Mizutani, F. Application of Integrated SECM Ultra-Micro-Electrode and AFM Force Probe to Biosensor Surfaces. *Bioelectrochem.* **2004**, *63*, 217–224.
26. Fasching, R. J.; Tao, Y.; Prinz, F. B. Cantilever Tip Probe Arrays for Simultaneous SECM and AFM Analysis. *Sens. Actuators, B* **2005**, *108*, 964–972.
27. Davoodi, A.; Farzadi, A.; Leygraf, C.; Zhu, Y. Developing an AFM-Based SECM System; Instrumental Setup, SECM Simulation, Characterization, and Calibration. *J. Electrochem. Soc.* **2008**, *155*, C474–C485.
28. Pierce, D. T.; Unwin, P. R.; Bard, A. J. Scanning Electrochemical Microscopy. 17. Studies of Enzyme-Mediator Kinetics for Membrane- and Surface-Immobilized Glucose Oxidase. *Anal. Chem.* **1992**, *64*, 1795–1804.
29. Pierce, D. T.; Bard, A. J. Scanning Electrochemical Microscopy. 23. Retention Localization of Artificially Patterned and Tissue-Bound Enzymes. *Anal. Chem.* **1993**, *65*, 3598–3604.
30. Wipf, D. O.; Bard, A. J. Scanning Electrochemical Microscopy. Part 7. Effect of Heterogeneous Electron-Transfer Rate at the Substrate on the Tip Feedback Current. *J. Electrochem. Soc.* **1991**, *138*, 469–474.
31. Hoeben, F. J. M.; Meijer, F. S.; Dekker, C.; Albracht, S. P. J.; Heering, H. A.; Lemay, S. G. Toward Single-Enzyme Molecule Electrochemistry: [NiFe]-Hydrogenase Protein Film Voltammetry at Nanoelectrodes. *ACS Nano* **2008**, *2*, 2497–2504.
32. Bard, A. J. Toward Single Enzyme Molecule Electrochemistry. *ACS Nano* **2008**, *2*, 2437–2440.
33. *The Enzymes*; Sigman, D. S., Ed.; Academic Press: San Diego, CA, 1992; Vol. 12, pp 150−155.
34. Anne, A.; Demaille, C.; Goyer, C. Electrochemical Atomic-Force Microscopy Using a Tip-Attached Redox Mediator. Proof-of-Concept and Perspectives for Functional Probing of Nanosystems. *ACS Nano* **2009**, *3*, 349–353.
35. Anicet, N.; Anne, A.; Bourdillon, C.; Demaille, C.; Moiroux, J.; Savéant, J. M. Electrochemical Approach to the Dynamics of Molecular Recognition of Redox Enzyme Sites by Artificial Cosubstrates in Solution and in Integrated Systems. *Faraday Discuss.* **2000**, *116*, 269–279.

36. Anne, A.; Demaille, C.; Moiroux, J. Elastic Bounded Diffusion and Electron Propagation. Dynamics of the Wiring of a Self-Assembly of Immunoglobulins Bearing Terminally Attached Ferrocene Poly(ethylene glycol) Chains According to a Spatially Controlled Organization. *J. Am. Chem. Soc.* **2001**, *123*, 4817–4825.
37. Hecht, H. J.; Kalisz, H. M.; Hendle, J.; Schmid, R. D.; Schomburg, D. Crystal Structure of Glucose Oxidase from *Aspergillus niger* Refined at 2 · 3 Å. Resolution. *J. Mol. Biol.* **1993**, *229*, 153–172.
38. Anne, A.; Moiroux, J. Quantitative Characterization of the Flexibility of Poly(ethylene glycol) Chains Attached to a Glassy Carbon Electrode. *Macromolecules* **1999**, *32*, 5829–5835.
39. Anne, A.; Demaille, C.; Moiroux, J. Terminal Attachment of Polyethylene Glycol (PEG) Chains to a Gold Electrode Surface. Cyclic Voltammetry Applied to the Quantitative Characterization of the Flexibility of the Attached PEG Chains and of Their Penetration by Mobile PEG Chains. *Macromolecules* **2002**, *35*, 5578–5586.
40. Gabriel, S.; Jerôme, C.; Jerôme, R.; Fustin, C. A.; Pallandre, A.; Plain, J.; Jonas, A. M.; Duwez, A. S. One-Step Polymer Grafting from Silicon Nitride SPM Probes: From Isolated Chains to Brush Regime. *J. Am. Chem. Soc.* **2007**, *129*, 8410–8411.
41. Israelachvili, J. *Intermolecular and Surface Forces*, 2nd ed.; Academic Press: San Diego, CA, 1992; pp 288−311.
42. Dolan, A. K.; Edwards, S. F. Theory of the Stabilization of Colloids by Adsorbed Polymer. *Proc. R. Soc. London, Ser. A* **1974**, *337*, 509–516.
43. Garnier, L.; Gauthier-Manuel, B.; van der Vegte, E. W.; Snijders, J.; Hadziioannou, G. Covalent Bond Force Profile and Cleavage in a Single Polymer Chain. *J. Chem. Phys.* **2000**, *113*, 2497–2503.
44. *Applied Scanning Probe Methods*; Bhushan, B., Fuchs, H., Hosaka, S., Eds.; Springer Verlag: Berlin, 2004.
45. Navarre, S.; Choplin, F.; Bousbaa, J.; Bennetau, Nony, L.; Aimé, J. P. Structural Characterization of Self-Assembled Monolayers of Organosilanes Chemically Bonded onto Silica Wafers by Dynamical Force Microscopy. *Langmuir* **2001**, *17*, 4844–4850.
46. Martin, P.; Marsaudon, S.; Thomas, L.; Desbat, B.; Aimé, J. P.; Bennetau, B. Liquid Mechanical Behavior of Mixed Monolayers of Amino and Alkyl Silanes by Atomic Force Microscopy. *Langmuir* **2005**, *21*, 6934–6943.
47. Nnebe, I. M.; Schneider, J. W. Tapping-Mode AFM Study of the Compression of Grafted Poly(ethylene glycol) Chains. *Macromolecules* **2006**, *39*, 3616–3621.
48. Kenworthy, A. K.; Hristova, K.; Needham, D.; McIntosh, T. J. Range and Magnitude of the Steric Pressure between Bilayers Containing Phospholipids with Covalently Attached Poly(ethylene glycol). *Biophys. J.* **1995**, *68*, 1921–1936.
49. Bar, G.; Delineau, L.; Brandsch, R.; Ganter, M.; Whangbo, M. H. Hysteresis in the Distance-Sweep Curves of Elastomers and its Implications in Tapping Mode Atomic Force Microscopy. *Surf. Sci.* **2000**, *457*, L404–L412.
50. Kueng, A.; Kranz, C.; Mizaikoff, B.; Lugstein, A.; Bertagnolli, E. Combined Scanning Electrochemical Atomic Force Microscopy for Tapping Mode Imaging. *Appl. Phys. Lett.* **2003**, *82*, 1592–1594.
51. Chang, H.; Bard, A. J. Observation and Characterization by Scanning Tunneling Microscopy of Structures Generated by Cleaving Highly Oriented Pyrolytic Graphite. *Langmuir* **1991**, *7*, 1143–1153.
52. McCreery, R. L. Advanced Carbon Electrode Materials for Molecular Electrochemistry. *Chem. Rev.* **2008**, *108*, 2646–2687.
53. Frederix, P. L. T. M.; Bosshart, P. D.; Akiyama, T.; Chami, M.; Gullo, M. R.; Blackstock, J. J.; Dooleweerdt, K.; de Rooij, N. F.; Staufer, U.; Engel, A. Conductive Supports for Combined AFM-SECM on Biological Membranes. *Nanotechnology* **2008**, *19*, 384004.
54. Williams, C. G.; Edwards, M. A.; Colley, A. L.; Macpherson, J. V.; Unwin, P. R. Scanning Micropipet Contact Method for High-Resolution Imaging of Electrode Surface Redox Activity. *Anal. Chem.* **2009**, *81*, 2486–2495.
55. Fan, F. R. F.; Bard, A. J. Electrochemical Detection of Single Molecules. *Science* **1995**, *267*, 871–874.
56. Fan, F. R. F.; Juhyoun Kwak, J.; Bard, A. J. Single Molecule Electrochemistry. *J. Am. Chem. Soc.* **1996**, *118*, 9669–9675.
57. Sun, P.; Mirkin, M. V. Electrochemistry of Individual Molecules in Zeptoliter Volumes. *J. Am. Chem. Soc.* **2008**, *130*, 8241–8250.
58. Stroh, C.; Wang, H.; Bash, R.; Ashcroft, B.; Nelson, J.; Gruber, H.; Lohr, D.; Lindsay, S. M.; Hinterdorfer, P. Single-Molecule Recognition Imaging Microscopy. *Proc. Natl. Acad. Sci. U.S.A.* **2004**, *101*, 12503–12507.
59. Kienberger, F.; Ebner, A.; Gruber, H. J.; Hinterdorfer, P. Molecular Recognition Imaging and Force Spectroscopy of Single Biomolecules. *Acc. Chem. Res.* **2006**, *39*, 29–36.
60. Vincent, G.; Haïdar, R.; Collin, S.; Guérineau, N.; Primot, J.; Cambril, E.; Pelouard, J.-L. J. Realization of Sinusoidal Transmittance with Subwavelength Metallic Structures. *Opt. Soc. Am. B* **2008**, *25*, 843.
61. Ghilane, J.; Hapiot, P.; Bard, A. J. Metal/Polypyrrole Quasi-Reference Electrode for Voltammetry in Nonaqueous and Aqueous Solutions. *Anal. Chem.* **2006**, *78*, 6868–6872.